Available online at www.sciencedirect.com
SCIENCE DIRECT
Polymer 47 (2006) 319–329
polymer
www.elsevier.com/locate/polymer

Large deformation rate-dependent stress–strain behavior of polyurea and polyurethanes

J. Yi [a], M.C. Boyce [a,*], G.F. Lee [a], E. Balizer [b]

[a] Department of Mechanical Engineering, Massachusetts Institute of Technology, Cambridge, MA 02139, USA
[b] Naval Surface Warfare Center, Silver Spring, MD 20903, USA

Received 5 August 2005; received in revised form 20 October 2005; accepted 23 October 2005
Available online 21 November 2005

Abstract

The thermoplastic elastomer polyurethane and the elastomeric thermoset polyurea are finding new applications in increasing the survivability of structures under impact loading, including those encountered in blast and ballistic events. However, the mechanical behavior of polyurea and polyurethane materials under these high rate conditions is relatively unknown. Here, the rate-dependent stress–strain behavior of one polyurea and three representative polyurethane materials is studied by dynamic mechanical analysis, quasi-static compression testing and split Hopkinson pressure bar (SHPB) testing. The polyurethane chemistries were chosen to probe the influence of the hard segment content on the mechanical behavior, where the volume fraction and the amorphous vs. crystalline structure of the hard segment domains were varied. The large strain stress–strain behavior of polyurea and polyurethane shows strong hysteresis, cyclic softening, and strong rate-dependence. The polyurethane with a non-crystalline well-dispersed hard segment morphology did not exhibit cyclic softening. The materials are observed to transition from a rubbery-like behavior under low strain rate ($\sim 10^{-3}$–$10^{0}\ s^{-1}$) loading conditions to either a leathery or glassy-like behavior under high strain rate ($\sim 10^{-3}\ s^{-1}$) loading conditions.

Keywords: Rate-dependence; Stress–strain behavior; Polyurethane

1. Introduction

Introduced by Otto Bayer in 1937 as a replacement for rubber, polyurethane has become one of the most versatile materials today. Within the polyurethane family, thermoplastic polyurethane (TPU) has been an attractive polymeric material because of the ability to alter its microstructure and thus its mechanical behavior. TPU offers a myriad of physical property combinations and processing applications [1–5]. It is highly elastic, flexible and resistant to abrasion, impact and weather.

TPU is a linear segmented block copolymer composed of 'hard' segments with a high T_g or a high T_m and 'soft' segments with a low T_g. The soft segment has its glass transition below the normal operating temperature and is, therefore, rubbery. The hard segment has its glass transition or its melting temperature above the ordinary operating temperature and is, therefore, either glassy and/or crystalline. Since the soft and hard segments are chemically dissimilar, they tend to phase separate forming a microstructure at the tens of nanometer length scale as shown, for example, in the atomic force microscope images of Aneja and Wilkes [5]. The hard segment domains are typically dispersed in a soft segment matrix and often form a spherulitic structure. Either one phase or both phases can be crystalline [6]. It is well known that the microphase separation of 'hard' and 'soft' domains is responsible for the versatile properties of this broad class of polymer [1–5].

The mechanical behavior of TPU has been studied by several groups in the past. Russo and Thomas [7] researched a series of polyurethanes with different percent of hard segment by mechanical testing at low strain rate. They found that an increase in hard segment content results in an increase in initial modulus, an increase in ultimate strength, and a decrease in elongation to break. O'Sickey et al. [4] evaluated the mechanical properties of poly(urethane urea) over a narrow range (6.3 and 9 wt%) of hard segment content and found that the hard segment content has little effect on the morphology and soft segment mechanical properties over this range in chemistry alteration. Sharma et al. [8] conducted a high strain rate compression test (SHPB) on a polyurethane,

* Corresponding author. Tel.: +1 617 253 5087.
E-mail address: mcboyce@mit.edu (M.C. Boyce).

0032-3861/$ - see front matter © 2005 Elsevier Ltd. All rights reserved.
doi:10.1016/j.polymer.2005.10.107

showing a single stress–strain curve at one strain rate ($1612\ s^{-1}$) to a maximum strain of -0.2. Qi and Boyce [9] conducted a systematic experimental study on the large strain stress–strain behavior of a TPU at low strain rates documenting the time dependence of the behavior as well as the strain-induced softening. Qi and Boyce [9] presented a review of the connections between morphology and mechanical properties in TPUs and then proposed a constitutive model for the observed behavior. Prisacariu et al. [10] recently reported a systematic investigation on the effect of varying hard and soft segment chemistry, crosslinking and preparation procedures, on the mechanical response of melt-cast MDI- and DMDI-based polyurethane elastomers. They concluded that DBDI-based (or partially DBDI-based) polyurethane has a higher flow stress in the hard phase, caused by more complete phase segregation and the hard phase crystallinity. The large strain tensile tests of Prisacariu and co-workers [10] clearly indicated some of the major mechanical features of TPU, including hysteresis and cyclic softening (up to the second cycle). Very recently, polyurethane is finding new applications in increasing the survivability of structures under impact loading, including blast and ballistic loading events. A thorough understanding of the stress–strain behavior of polyurethane over a wide range of strain rates becomes necessary in order to understand the behavior during normal operating conditions as well as during impact events.

In this paper we report a series of tests to study the dependence of the mechanical behavior, from small to large strain, over a wide range of strain rates, including dynamic mechanical analysis to understand the shift in the glass transition temperature with strain rate, quasi-static compression testing and split-Hopkinson pressure bar testing following the experimental protocol of Mulliken and Boyce [11,12] which was used to correlate molecular transition regimes with high strain rate behavior in glassy polymers. Three representative polyurethane samples of varying hard segment content and chain extender, and one polyurea, are studied.

2. Experimental protocol

2.1. Materials

The polyurea and three polyurethane materials tested in this research were prepared at Naval Surface Warfare Center. The polyurea was based on multifunctional isocyanate (functionality 2.4) (Isonate 2143L) and high molecular weight diamine (Versalink P1000), while the polyurethanes were based on diphenylmethane diisocyanate (MDI, ISONATE™ 143L, from Dow Chemical, Midland, Michigan), and poly(tetramethylene ether) glycol (PTMG, Terathane® 1000, INVISTA, Wichita, KS), mixed with chain extender, 1, 4-butanediol (BDO, Sigma-Aldrich, St Louis, MO) or 2,2-dimethyl-1,3-propanediol (DMPD, Sigma-Aldrich, St Louis, MO). Table 1 lists the composition of the polyurea and three polyurethanes in this paper. The composition of polyurethane was changed from sample to sample to provide different hard segment ratios. Sample PU1 possessed a 54% hard segment content; while sample PU2 and PU3 possessed 55 and 44%, respectively. Sample PU2 was prepared with chain extender DMPD, instead of 1,4-BDO in PU1 and PU3. Polyurethanes containing a pendant group, such as, DMPD, in chain extender yield non-crystalline hard segments and better phase mixing [6]. Those polyurethanes containing 1,4-BDO have a crystalline hard segment. Materials were prepared as compression molded sheets with a thickness of about 6 mm. Specimens for mechanical testing were cut from the sample sheets.

Table 1
Polyurethane samples composition

Sample	Chain extender			
	MDI (mol%)	PTMG (mol%)	1,4-BDO (mol%)	DMPD (mol%)
Polyurea	–	–		
PU1	50	16.7	33.3	
PU2	50	16.7		33.3
PU3	50	25	25	

Tapping mode atomic force microscopy (Digital Instruments Multimode Scanning Probe Microscope) was utilized in attempts to image the microstructure. Initially, the surface of freshly cut specimens were examined with AFM. However, no clear features were observed at any length scale. Solution cast films of PU1 and PU2 were then prepared. In PU1, spherulitic or spherulitic-like domains of diameter 1–3 μm were observed with internal hard/soft phase of around 10 nm. In PU2, no discernable features were observed[1].

2.2. Dynamic mechanical analysis

Dynamic mechanical analysis (DMA) was performed on a TA Instruments Q800 Dynamic mechanical analyzer. Specimens of rectangular geometry were machined with a width of 3 mm, a thickness of 2 mm and a gauge length of around 9 mm. The specimens were tested in uniaxial tension at a fixed frequency of 1 Hz and a strain amplitude of 0.1% from -156 to 80 °C with a heating rate of 3 °C/min.

The oscillatory strain history of the DMA test means the strain rate that the specimen experiences also varies over the course of the strain history. It is useful to express the frequency dependence of the DMA data as a strain rate dependence. Thus, an equivalent average strain rate is computed from the test frequency and the strain amplitude. By approximating the applied sinusoidal strain wave with a triangular strain wave,

[1] We note that the solution cast film might have a different phase morphology than the compression molded sheet of polyurethane. The solution cast AFM sample was made only after the un-successful attempts to reveal the hard/soft phase morphology using cryotomed cross-sections of bulk PU1 and PU2. Secondly, the AFM observations were made on the free surface of the solution cast film. The morphology observed on the free surface might also be different than the bulk morphology.

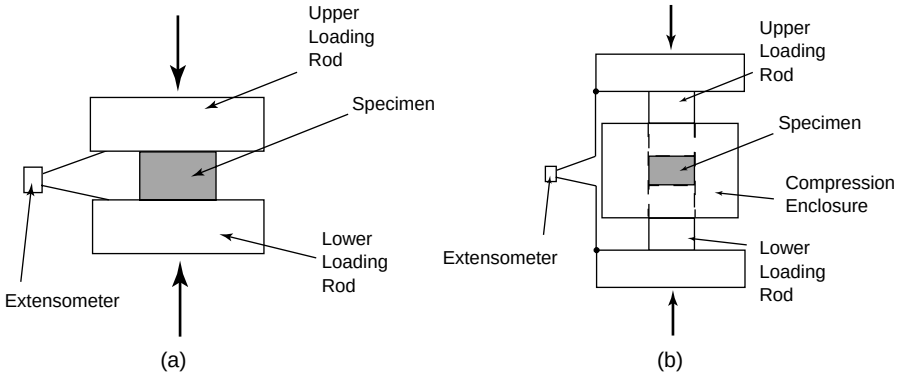

Fig. 1. Schematic drawings of uniaxial compression tests (a) un-confined (b) confined.

the equivalent average strain rate can be calculated as, $\dot{\varepsilon} = 2\varepsilon\omega$, where $\dot{\varepsilon}$ is the equivalent strain rate, ε is the strain amplitude, and ω is the test frequency.

Additional tests were conducted at 1, 10 and 100 Hz at a strain amplitude of 0.1% corresponding to the equivalent strain rates of 2×10^{-3}, 2×10^{-2} and 2×10^{-1} s^{-1}, respectively, to identify any shifts in transition regimes with strain rates.

2.3. Quasi-static compression tests

The large strain stress–strain behavior in the quasi-static regime is evaluated by constant strain rate uniaxial compression tests (Fig. 1(a)). The compression specimens measured 12 mm in diameter and about 6 mm in height. Most of the tests were conducted on an Instron 1350 servo-hydraulic axial testing machine using a true strain rate control mode, while some were conducted on a Zwick screw drive axial testing machine using an engineering strain rate control mode. For Instron tests, the actuator displacement is controlled by a constant true strain rate wave form generated by a computer with a LabView testing program. Specimen height was monitored using an extensometer and was used in the feedback loop with the actuator. For Zwick tests, the actuator displacement is controlled by a constant engineering strain rate wave form generated by a computer with Zwick testXpert® testing software. Specimen height was measured

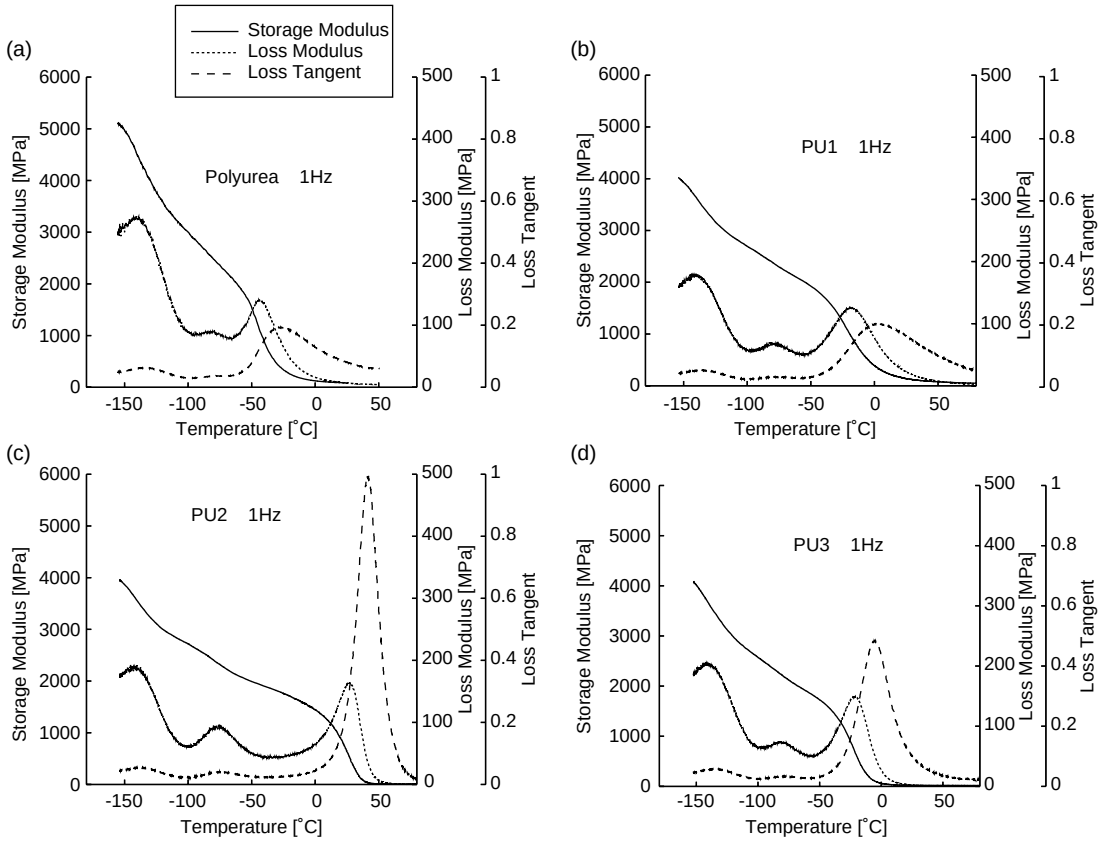

Fig. 2. DMA results of storage modulus, loss modules, and loss tangent for (a) polyurea, (b) PU1, (c) PU2 (d) PU3 at a frequency of 1 Hz (equivalent average strain rate of 2×10^{3} s^{-1}).

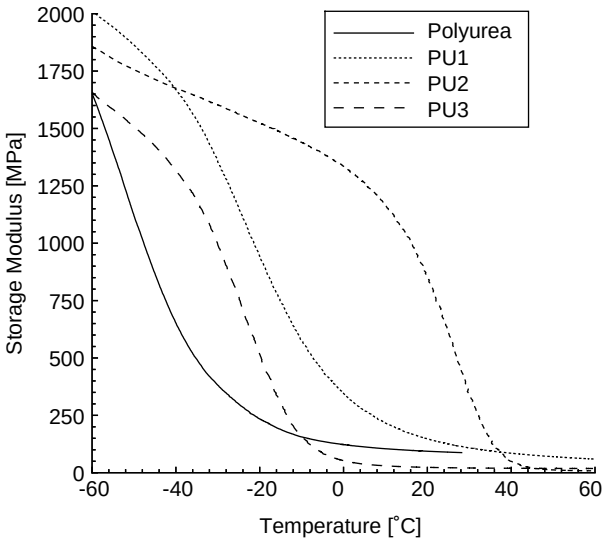

Fig. 3. DMA results of storage modulus in glass transition regime for polyurea, PU1, PU2, PU3 at a frequency of 1 Hz (equivalent average strain rate of $2\times10^{3}\ s^{-1}$).

by the displacement of the crosshead and was also used in the feedback loop with the actuator. In both machines, specimens were compressed between hardened steel compression platens containing a spherical seat to overcome any small misalignment along the load train. Lubrication was applied on the surfaces of both upper and lower platens. A sheet of teflon foil was also inserted between the specimen and the layer of lubrication to further eliminate friction and prevent inhomogeneous deformation.

Confined compression tests (Fig. 1(b)) were conducted on an Instron testing machine on the polyurea and polyurethane samples. A stainless steel enclosure with an internal diameter close to the test samples' outer diameter plus a very small tolerance was used to restrict the lateral movement of the samples. The size of the cylindrical samples is about 12 mm in diameter, 6 mm in thickness. The outer diameter of the enclosure is 30 mm. Two loading rods were machined to fit within the enclosure with a rather small tolerance. The axial deformation of the sample is monitored by the extensometer fixed on the upper and lower loading platens as in the un-confined tests. This test provides a nearly pure hydrostatic pressure loading condition and a measure of the bulk modulus of each material. For small strain, linear isotropic elasticity, the slope of the axial stress vs. axial strain curve will be:

$$M_{\text{confined}} = \frac{E(1-\nu)}{(1-2\nu)(1+\nu)} \tag{1}$$

Recall the bulk modulus $B = E/3(1-2\nu)$; therefore, for a material with a Poisson ratio close to 0.5, this slope is essentially close to B. Otherwise, M_{confined} can be used with E from the uniaxial experiment to get B.

2.4. High strain rate compression tests

High strain rate compression testing was performed on a split-Hopkinson pressure bar apparatus designed in cooperation with and built by Physics Applications, Inc. of Dayton, OH (see Mulliken and Boyce [12]). This apparatus employs solid aluminum pressure incident and transmission bars, both with a length of about 2.3 m and a diameter of 19.05 mm. The specimens were of a cylindrical geometry with diameter of 4 mm and thickness of 2 mm. The thickness-to-diameter ratio of 1:2 and relatively small thickness are necessary to minimize wave attenuation [14]. The thickness-to-diameter ratio of 1:2 has also been shown to minimize the effects of radial and longitudinal inertia in the specimen. A thin layer of petroleum jelly was applied on both sides of the specimen and the end faces of the incident bar and the transmission bar to lubricate the contact surfaces, so that a homogeneous deformation state is achieved. A digital oscilloscope, Gage scope (Gage Applied Technologies, Que., Canada) having a $50\times10^{6}\ s^{-1}$ sampling rate capacity, was used to collect the testing data. The pulse shaping technique was not employed in these tests. Due to the nature of applying deformation to a specimen in SHPB testing, there is typically an increase in strain rate over the course of the deformation; thus, we report both the history of the axial strain rate as a function of axial strain and the axial stress as a function of axial strain.

3. Experimental results

3.1. Dynamic mechanical analysis (DMA)

DMA results for storage modulus, loss modulus and loss tangent at a frequency of 1 Hz over a temperature range of

Table 2
Polyurethane sample properties

Sample	Density (g/mm^3)	Hard segment (wt%)	Chain extender	T_g (°C) DSC	T_g (°C) DMA @ 1 Hz	T_g shift (°C/decade strain rate)	T_β (°C)	T_γ (°C)
Polyurea	1.1	37	–	–	−47	4.0	−80	−141
PU1	1.140	54	1,4-BDO	−38	−17	4.6	−75	−140
PU2	1.128	55	DMPD	12	24	4.7	−80	−146
PU3	1.133	44	1,4-BDO	−37	−25	4.6	−80	−144

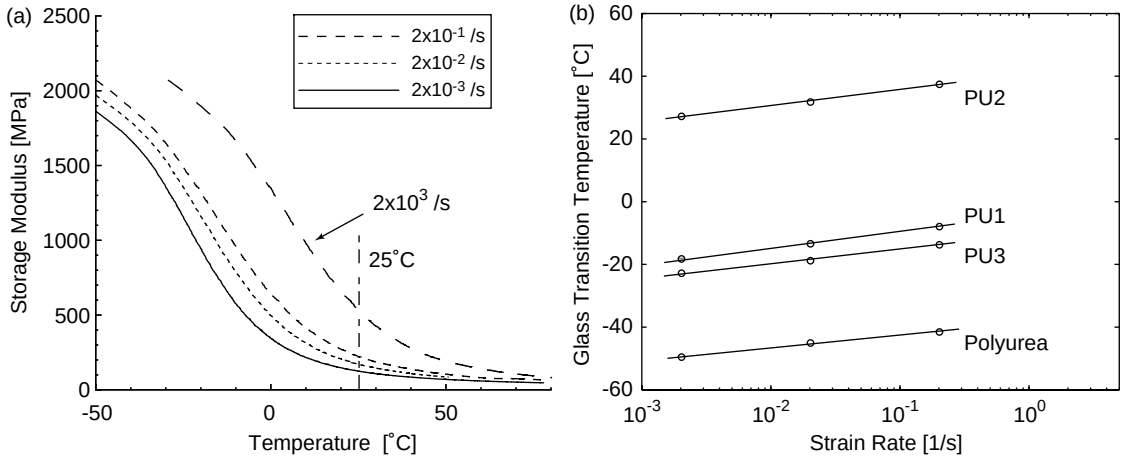

Fig. 4. The shifting effect with strain rate: (a) storage modulus shift with strain rate of sample PU1, including an extrapolated storage modulus curve at a strain rate of $2\times10^3\ s^{-1}$, (b) glass transition temperature shift with strain rate for all four samples.

−156−80 °C (50 °C for polyurea sample) are plotted in Fig. 2. Fig. 3 plots a portion of the storage modulus curve for each material in its glass transition regime (at 1 Hz) for comparison purposes. Three transitions are observed in these plots: the primary alpha or glass transition at −47 °C for polyurea, −17 °C for PU1, 24 °C for PU2 and −25 °C for PU3; and two secondary transitions: a rather minor beta transition at −80 °C for Polyurea, at −75 °C for PU1, at −80 °C for PU2, and at −80 °C for PU3; and a more prominent gamma transition at −141 °C for polyurea,

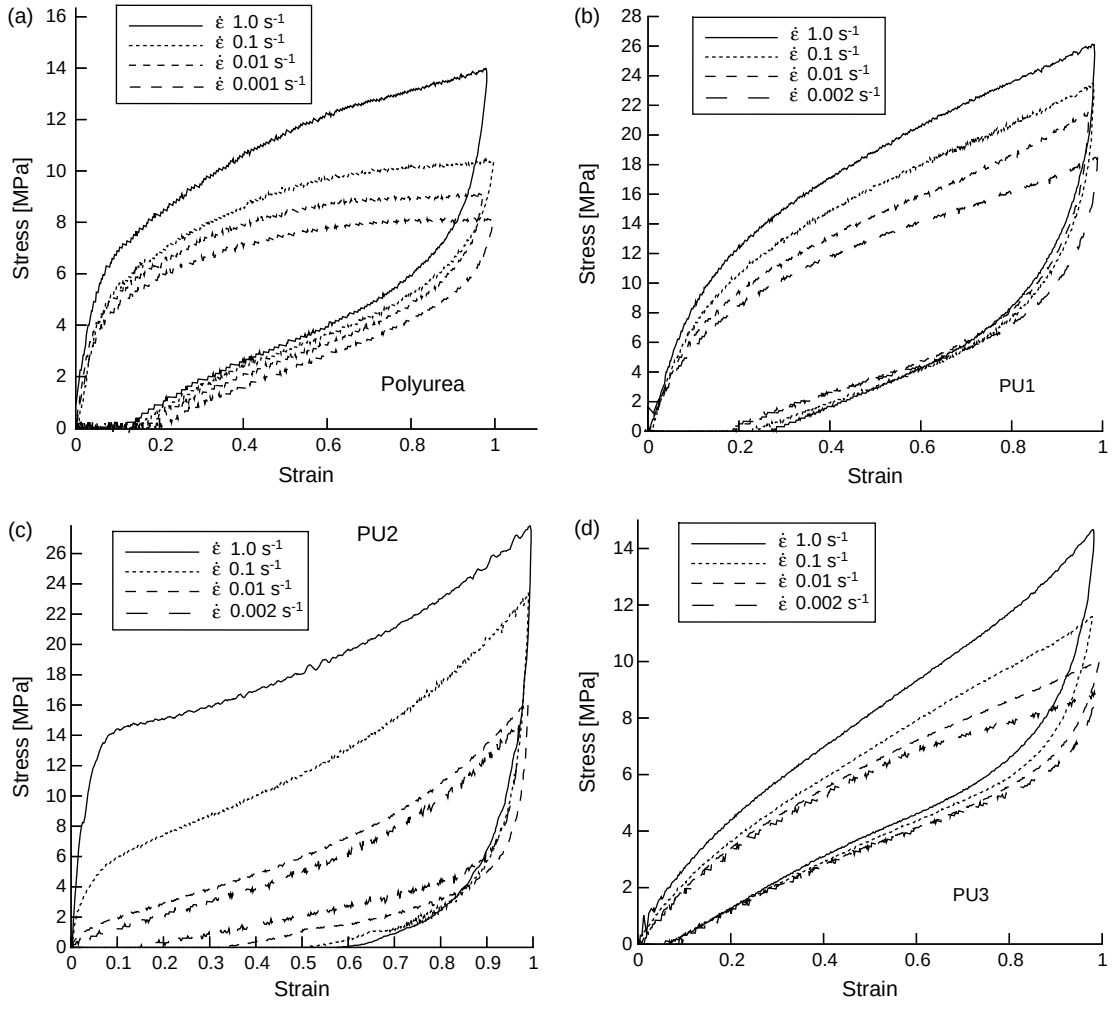

Fig. 5. Uniaxial compression stress–strain behavior of polyurethane in quasi-static strain rate regimes (a) polyurea, (b) PU1, (c) PU2, (d) PU3.

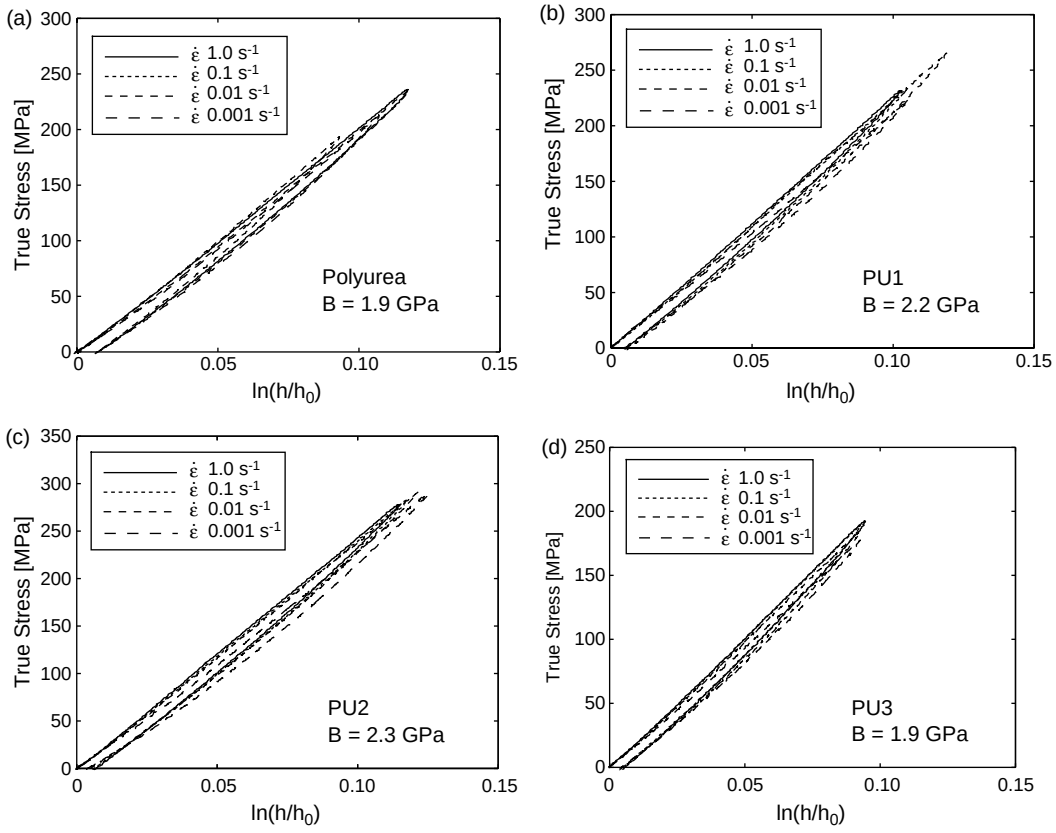

Fig. 6. Confined compression stress–strain behaviors of (a) polyurea, (b) PU1, (c) PU2, (d) PU3. The bulk modulus, B, for each material is obtained from these tests and listed in each plot.

−140 °C for PU1, −146 °C for PU2 and −144 °C for PU3. These data are also listed in Table 2. The high T_g of PU2 is presumably due to the fully dispersed/blended nature of the amorphous hard and amorphous soft segments (i.e. no clear phase segregation) giving a higher T_g than that of an isolated soft domain. The melting temperature of the hard domains is not seen in the plots because these DMA tests only sampled up to 80 °C. Typically, the hard domains melt at around 150 °C [7]. Differential scanning calorimetry (DSC) measurements were also conducted (Yi and Hsieh [17]) and the DSC-measured glass transition temperatures, T_g, are listed in Table 2.

The mechanical behavior is known to depend on strain rate as illustrated in sample PU3 shown in Fig. 4(a). The glass transition region of the storage modulus is observed to shift with strain rate in a linear manner over the tested range, as shown in Fig. 4(b) for all four samples. We signify this as a shift in 'apparent glass transition temperature', meaning the glass transition temperature that the material mechanically recognizes at the given strain rate. Table 2 lists the shift results for polyurea and PU1, PU2 and PU3. Extrapolating this linear relationship to the high strain rate regime, the temperature dependence of the modulus of these samples at high strain rates can be estimated; in particular, a transition into the leathery/glassy regime at room temperature 25 °C at the very high strain rates $\sim 10^3\ s^{-1}$ is observed (Fig. 4(c)).

3.2. Quasi-static large strain compression testing

3.2.1. Monotonic behavior at different strain rates

The large strain stress–strain behavior of all four materials is very non-linear as shown in Fig. 5. Here, true stress–true strain is used, where true stress is the load divided by current cross sectional area and true strain is the natural logarithm of the ratio of current height to initial height; current cross-sectional area was calculated assuming incompressible deformation. In the quasi-static regime (10^{-2}–$1\ s^{-1}$), the stress–strain behavior during loading and unloading was obtained and each sample demonstrates a hysteresis behavior. The initial stiffness has a very small dependence over this range in strain rate in polyurea, PU1 and PU3. However, sample PU2 demonstrated a rather dramatic change in stiffness over the low to moderate range in strain rates, transitioning from a rubbery-like behavior at $2\times10^{-3}\ s^{-1}$ to a leathery behavior at $1.0\ s^{-1}$. Similar phenomenon has been observed when testing PET and PETG around 80 °C (i.e. in their T_g regime) over this range in strain rates (Dupaix and Boyce [15]). In

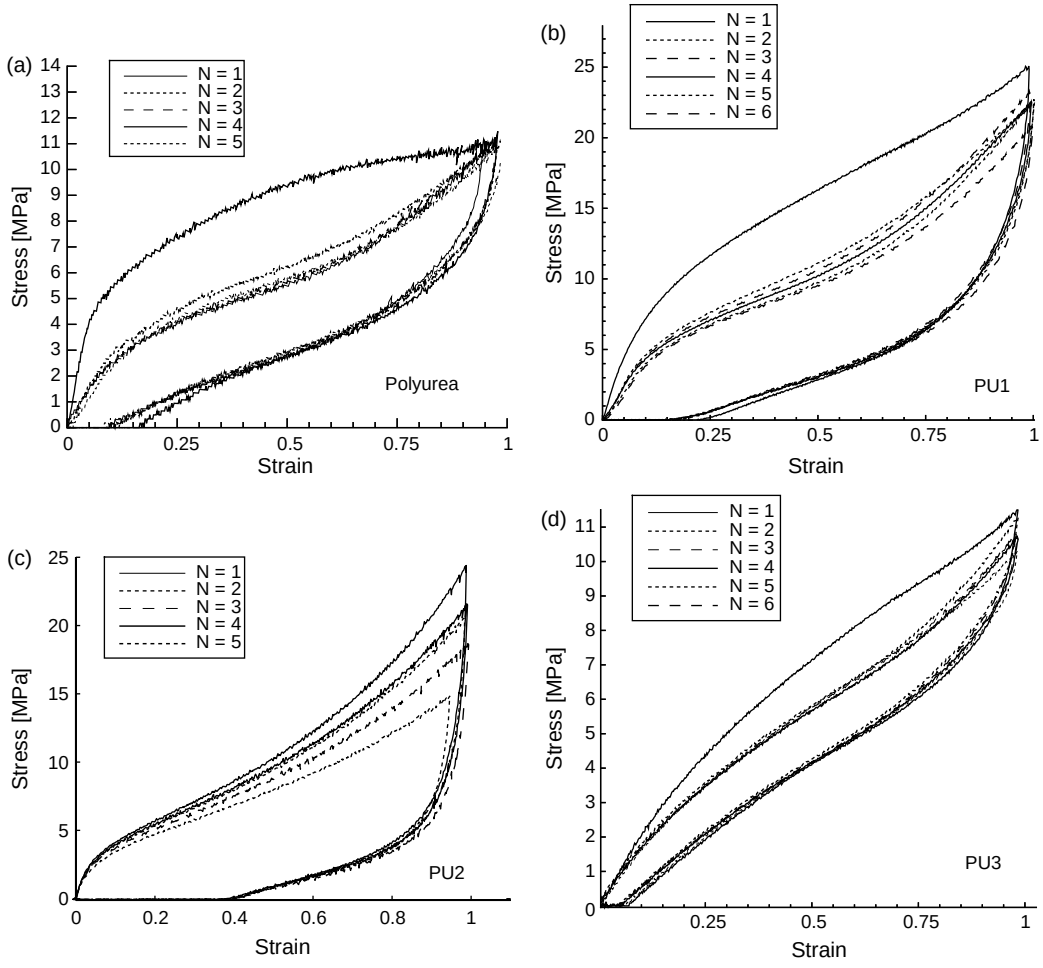

Fig. 7. Stress–strain behavior of three polyurethanes at cyclic uniaxial compression tests at strain rate $\dot{\varepsilon} = 0.1/\text{s}$. N indicates cycle numbers. (a) Polyurea, (b) PU1, (c) PU2, (d) PU3.

all materials, the rollover to flow is observed to be rate dependent, increasing with increases in strain rate. PU1 and PU2, with their greater hard segment content, have a higher initial stiffness, a higher roll-over stress level, a stronger rate dependence, and a greater hysteresis.

The unloading behavior is highly non-linear for all strain rates as shown in Fig. 5. PU1 and PU2 have a large residual strain, about -0.2 and -0.4, respectively, after an applied strain of -1.0, due to their high hard segment content; PU3 and polyurea have a residual strain of about -0.1 after an applied strain of -1.0. However, all of these residual strains were fully recovered within hours after the tests, including PU2, which has a relatively large residual strain at different rates.

The confined compression test on all 4 materials samples the hydrostatic behavior of the material and thus gives a much stiffer set of stress–strain curves as shown in Fig. 6. All curves had contained a small lead region until the specimen makes full radial contact with the confinement chamber; this region was removed from the data shown. The bulk modulus was evaluated at a strain of 0.05 for each material and is labeled on each plot. The bulk modulus for each material is ≈ 2 GPa.

3.2.2. Cyclic softening

Cyclic softening behavior is also observed in these samples by conducting consecutive loading-unloading-reloading on one specimen with a ~ 180 s time period in between each cycle[2], which was needed for re-measuring and re-positioning the specimen. Fig. 7 shows the uniaxial compression stress–strain behavior during cyclic tests to/from a strain of -1.0 at a true strain rate of $0.1\ \text{s}^{-1}$. The reloading stress–strain curves show a significantly more compliant character when compared to the initial loading behavior, with the exception of PU2, which essentially does not soften. Interestingly, PU1 (with a crystalline hard segment ratio of 54%) appears to soften to nearly the stress–strain behavior of PU2 (which has an amorphous hard segment ratio of 55%). The PU2 'softening' is quite different than that of the other materials, where only its large strain hardening stage is seen to soften and this may be more a result of the plasticity that occurs at this rate over this time period of cyclic loading rather than a softening of the rubbery behavior.

[2] There is a small (less than few percent) residual strain existing at the time of reloading after the ~ 180 s repositioning time. In the case without reloading, normally, this residual strain can be entirely removed in less than 1 hour.

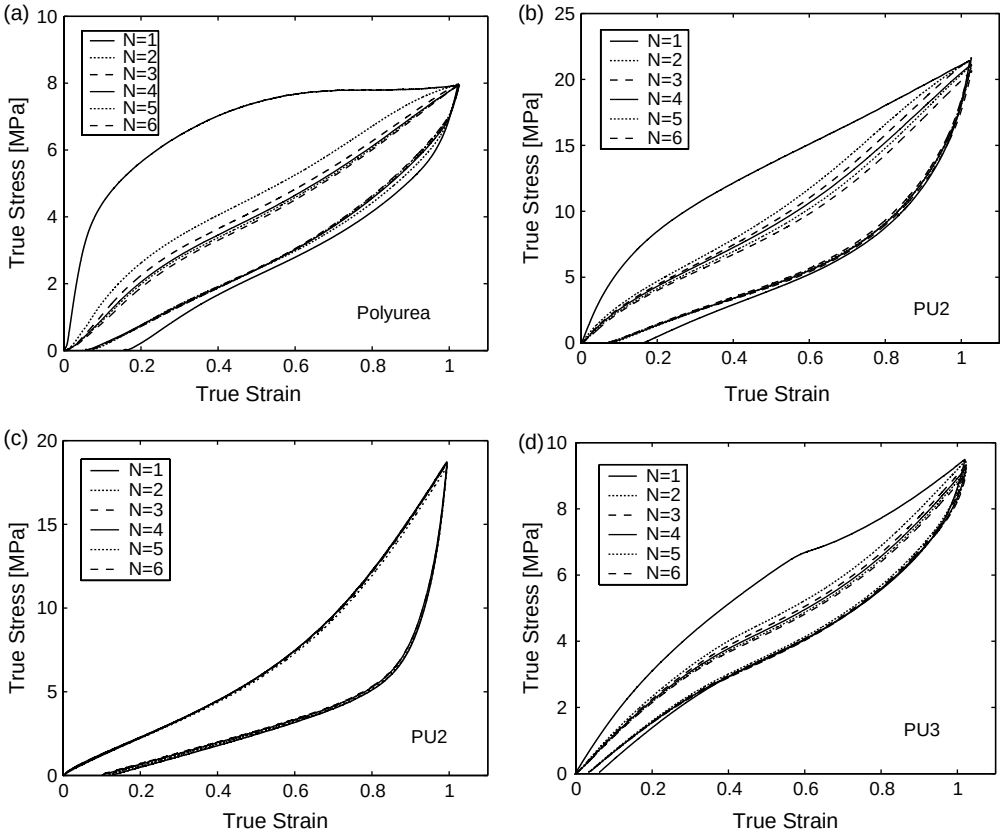

Fig. 8. Stress–strain behavior of three polyurethanes at cyclic uniaxial compression tests at engineering strain rate $\dot{\varepsilon} = 0.00126/s$. N indicates cycle numbers. (a) Polyurea, (b) PU1, (c) PU2, (d) PU3.

Note that strain-induced softening in TPU has been identified to be associated with the reorganization of the hard domain with strain (see, for example, Bonart and Muller-Riederer [16], Qi and Boyce [9]) The stress–strain cyclic loading curves also show that, after a few cycles, the stress–strain curves tend to stabilize to a fixed trajectory. Moreover, in PU1 and PU3, these curves demonstrate that even though there is a significant softening in the first few cycles, the unloading paths are relatively independent of cycle number, i.e., the unloading stress–strain behavior is not dependent on the deformation history. This has also been observed in the Qi and Boyce [9] data. Lastly, the residual strain is also not dependent on the deformation history.

In order to better understand whether the difference in PU2 softening behavior was due to its leathery regime at the $0.1\ s^{-1}$ rate or due to its amorphous hard segment content, cyclic tests were conducted at a lower strain rate of $0.00126\ s^{-1}$ (engineering strain rate) on all materials as shown in Fig. 8.

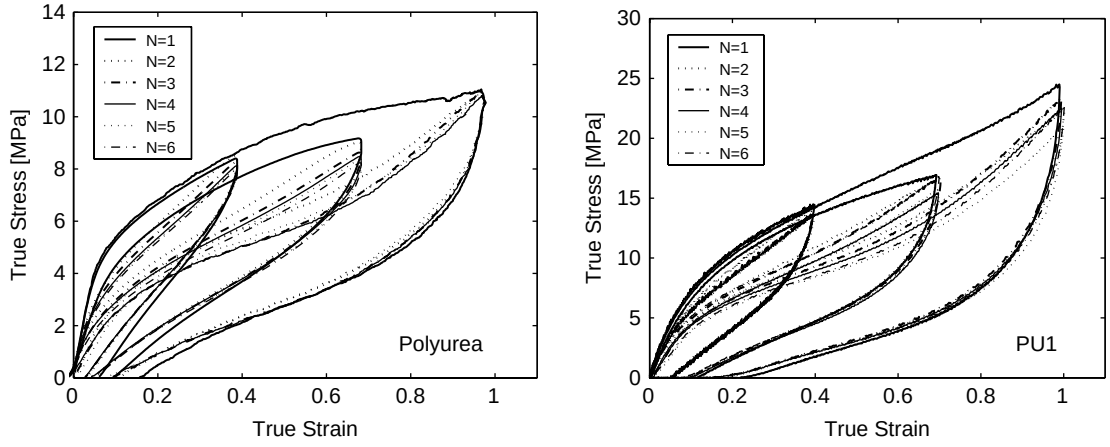

Fig. 9. Stress–strain behavior of three polyurethanes at cyclic uniaxial compression tests at engineering strain rate $\dot{\varepsilon} = 0.063/s$. N indicates cycle numbers. (a) Polyurea, (b) PU1.

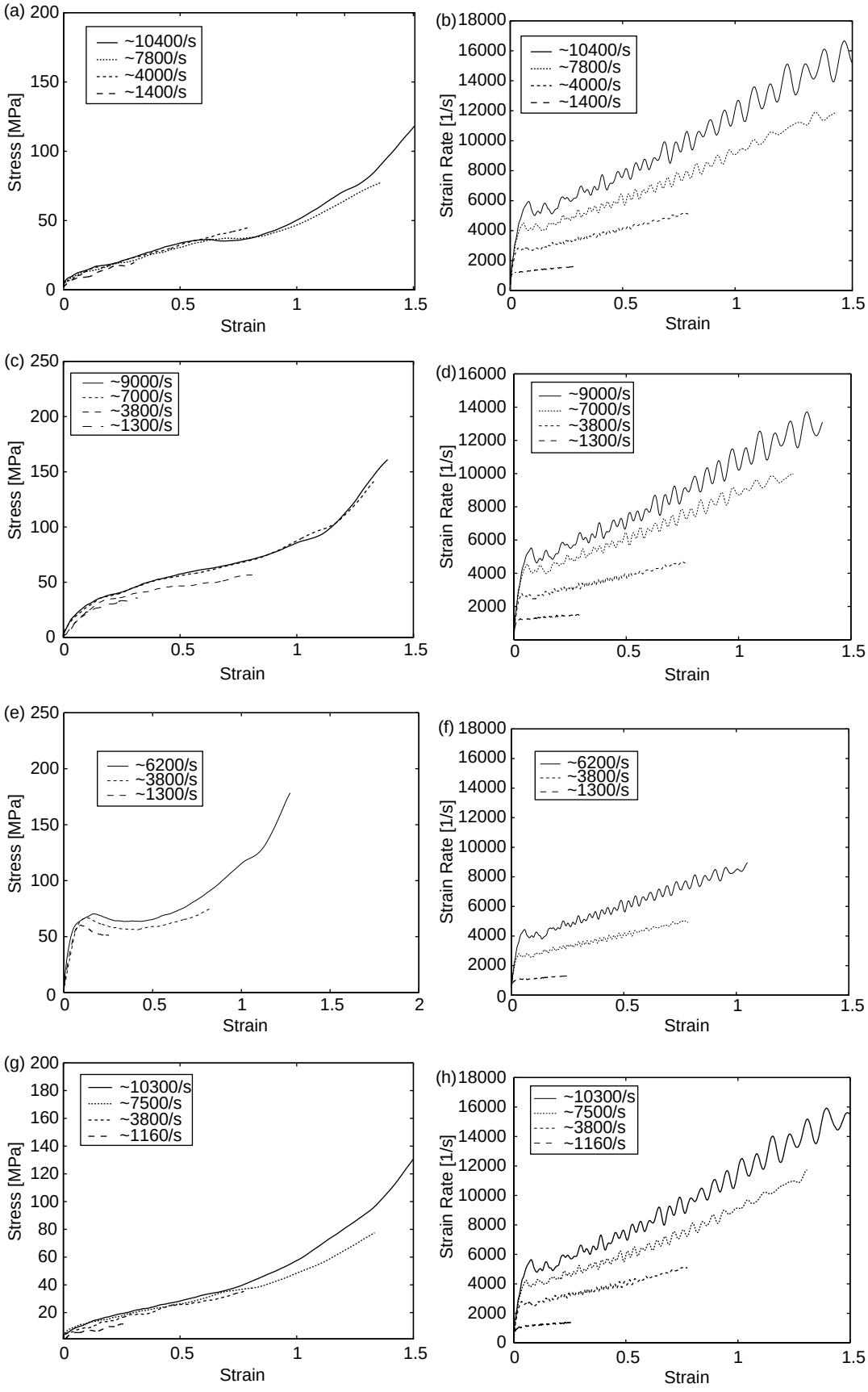

Fig. 10. Stress–strain behavior of polyurethane at high strain rate regimes and the corresponding true strain vs. strain rate curve (a, b) Polyurea, (c, d) PU1, (e, f) PU2, (g, h) PU3.

These data clearly show that PU2 does not exhibit cyclic softening in its rubbery regime. This suggests the amorphous nature of the PU2 hard segment content and its apparent lack of phase segregation, because of its composition with chain extender of DMPD, leads to this clear difference in behavior. This is consistent with the prior works (for example, Bonart, et al. [16]) which show cyclic softening to be related to breakdown/reorganization of segregated hard domains with strain.

Cyclic softening tests were also conducted at different strain level for polyurea and PU1 at same strain rate. Fig. 9 shows the stress–strain behavior at strain level of 0.4, 0.7 and 1.0. It shows that the softening behavior is strain-dependent. The 'stabilized' path depends on the amount of strain applied. The amount of softening also depends on the strain applied. The amount of softening increases with increasing strain. The unloading stress–strain behavior is independent of the strain cycle.

3.3. High strain rate large strain compression testing

In the high strain rate regime, the plots of true stress vs. true strain and strain rate vs. true strain of the SHPB tests are shown in Fig. 10. The initial stiffness region of the curves does not provide accurate data because the force acting on the front side and back side of the specimen takes $\sim$20 μs to reach dynamic equilibrium, which corresponds to -0.05 strain in most cases. The stress–strain behavior in the high strain rate regime ($\sim 10^3\ s^{-1}$) has a strong rate dependence. Fig. 11 plots the low to moderate stress–strain curves together with the high rate curves. In the polyurea and PU3 samples, the behavior transitions from a hysteretic rubbery behavior at low to moderate rates (0.001–1 s^{-1}) to a leathery behavior at high rates ($\sim 10^3\ s^{-1}$); PU2 transitions from a hysteretic rubbery-like behavior at low to moderate rates ((0.001–1 s^{-1}) to a nearly glassy behavior at high rates ($\sim 10^3\ s^{-1}$); and PU2 transitions to an entirely glassy behavior at high rates ($\sim 10^3\ s^{-1}$). A rollover to flow is observed at low strain, similar to the behavior at low strain rates shown in Fig. 5, however, at significantly higher stress level.

Fig. 12 presents the rate-dependence of the stress–strain behavior in a form of stress vs. logarithm strain rate, taking the stresses evaluated at strain levels of 0.15 and 0.30. For both strain levels, it clearly demonstrated a close-to-linear dependence on the logarithm of the strain rate in both the high strain rate ($> \sim 10^3\ s^{-1}$) and the low strain rate ($< \sim 10^0\ s^{-1}$) region. However, the linear relationship at high and low strain rate reveals that the rate dependence mechanism is different for high strain rates ($> \sim 10^3\ s^{-1}$) and low strain rate ($< \sim 10^0\ s^{-1}$), and potentially there is a temperature-dependent transition strain rate for different materials. This is consistent with the transition from a rubbery or leathery behavior at low rate to a leathery or glassy behavior at high rate (depending on the particular material).

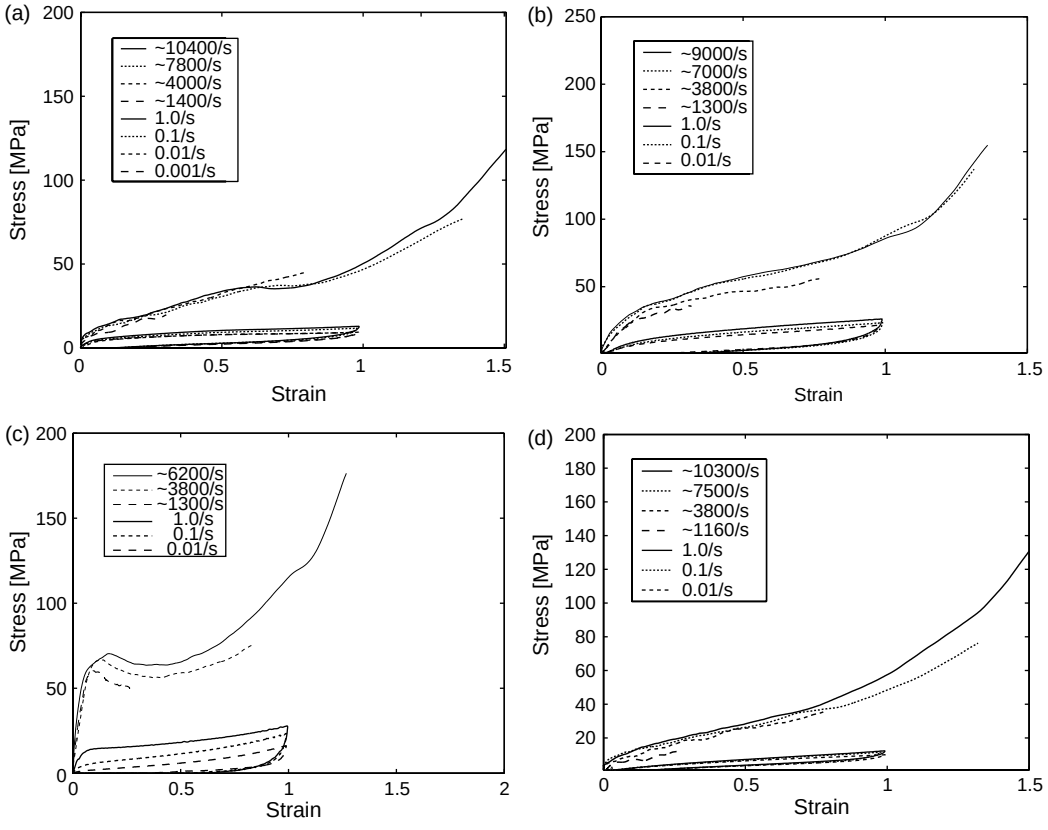

Fig. 11. Stress–strain behavior of polyurethane at quasi-static and high strain rate regimes (a) polyurea, (b) PU1, (c) PU2, (d) PU3.

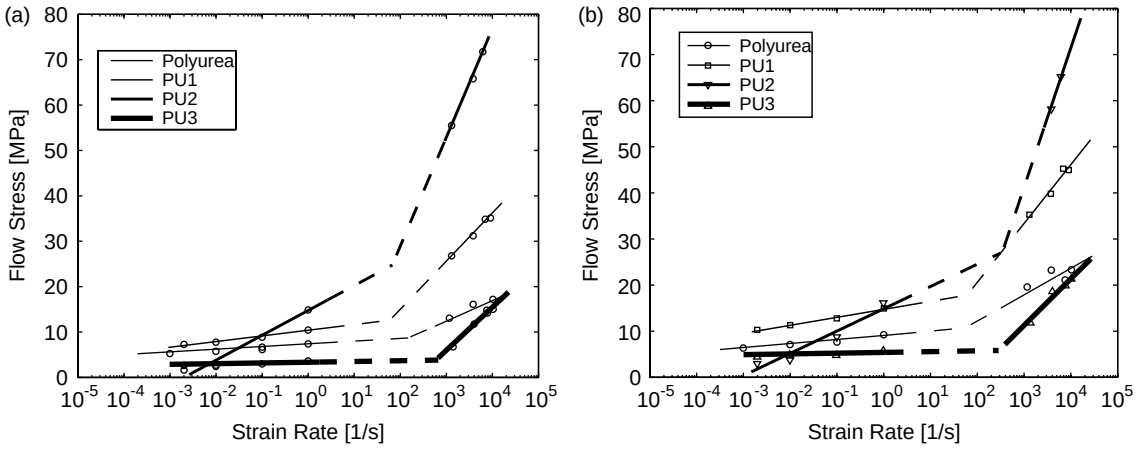

Fig. 12. Flow stress vs. strain rate of polyurea, PU1, PU2 and PU3 at strain (a) 0.15 and (b) 0.30.

4. Conclusion

Polyurea and three representative polyurethane samples with different hard segment ratio were examined by dynamic mechanical analysis and uniaxial compression tests in both the quasi-static and high strain rate regimes, from 10^3–10^4 s^{-1}. The glass transition temperature shift effect with strain rate is identified. The highly non-linear large strain stress–strain behavior demonstrates a strong hysteresis and rate dependent character. Cyclic softening was observed for these materials with a crystalline hard segment content and was absent for the material with an amorphous well-dispersed hard segment content. The polyurea, PU1 and PU2 materials are found to transition from a rubbery-like behavior at low strain rates ($\sim 10^3$–10^0 s^{-1}) to a glassy-like behavior at high strain rates ($\sim 10^3$ s^{-1}); the PU2 transitions from a leathery behavior to a glassy behavior. These data are consistent with the shift in mechanical T_g with strain rate which was identified in the DMA testing.

Acknowledgements

This research is funded by the Office of Naval Research through grant number N00014-04-10469. J. Yi appreciates Dr A. Hsieh of MIT Army Institute of Soldier Nanotechnology for DSC data, Ms S.M. Liff for making solution cast films, Dr S. Sarva and Mr A.D. Mulliken for the discussions and assistance in conducting SHPB tests. We acknowledge the contribution of Dr O. Samudrala and Prof S. Socrate in the initial stages of design and construction of the SHPB facility. We also acknowledge the use of the high rate experimental facilities at the MIT Army Institute of Soldier Nanotechnology. G.F. Lee and E. Balizer acknowledge the contribution of J. Fedderly for fabricating the materials.

References

[1] Schneider NS, Desper CR, Illinger JL, King AO, Barr D. J Macromol Sci Phys 1975;B11(4):527–52.
[2] Chen-Tsai CHY, Thomas EL, MacKnight WJ, Schneider NS. Polymer 1986;27(5):659–66.
[3] Garrett JT, Siedlecki CA, Runt J. Macromol 2001;34(20):7066–70.
[4] O'Sickey MJ, Lawrey BD, Wilkes GL. J Appl Polym Sci 2002;84(2):229–43.
[5] Aneja A, Wilkes GL. Polymer 2003;44(23):7221–8.
[6] Duffy JV, Lee GF, Lee JD, Hartmann B. Sound, vibration damping with polymers. In: Corsaro RD, Sperling LH, editors. ACS symposium series 424. Washington, DC: American Chemical Society; 1990. p. 281–300.
[7] Russo R, Thomas E. J Macromol Sci Phys 1983;B22(4):553–75.
[8] Sharma A, Shukla A, Prosser RA. J Mater Sci 2002;37(5):1005–17.
[9] Qi HJ, Boyce MC. Mech Mater 2005;37(8):817–39.
[10] Prisacariu C, Buckley CP, Caraculacu AA. Polymer 2005;46(11):3884–94.
[11] Mulliken AD, Boyce MC. Proceedings of the SEM conference on experimental mechanics 2004.
[12] Mulliken AD, Boyce MC. Int J Solids Struct, in press.
[14] Chen W, Zhang B, Forrestal MJ. Experim Mech 1999;39(2):81–5.
[15] Dupaix RB, Boyce MC. Polymer 2005;46(13):4827–38.
[16] Bonart R, Muller-Riederer G. Colloid Polym Sci 1981;259(9):926–36.
[17] Yi J, Hsieh A, Boyce MC. Submitted for publication.